International Journal of Pharmaceutics 419 (2011) 33–42

Contents lists available at ScienceDirect

International Journal of Pharmaceutics

journal homepage: www.elsevier.com/locate/ijpharm

Tissue slice model of human lung cancer to investigate telomerase inhibition by nanoparticle delivery of antisense 2′-O-methyl-RNA

Meng Dong[a], Claudia Philippi[b], Brigitta Loretz[b,c], Noha Nafee[b,1], Ulrich F. Schaefer[b], Godehard Friedel[d], Susanne Ammon-Treiber[a,e], Ernst-Ulrich Griese[a], Claus-Michael Lehr[b,c], Ulrich Klotz[a], Thomas E. Mürdter[a,*]

[a] Dr. Margarete Fischer-Bosch-Institute of Clinical Pharmacology, Stuttgart and University of Tübingen, Germany
[b] Department of Biopharmaceutics and Pharmaceutical Technology, Saarland University, Saarbrücken, Germany
[c] Department Drug Delivery, Helmholtz-Institute for Pharmaceutical Research Saarland (HIPS), Helmholtz Center for Infectious Research (HZI), Saarland University, Saarbrücken, Germany
[d] Department of Thoracic Surgery, Schillerhoehe Hospital, Gerlingen, Germany
[e] Department of Clinical Pharmacology, University Hospital Tübingen, Tübingen, Germany

ARTICLE INFO

Article history:
Received 21 April 2011
Received in revised form 5 July 2011
Accepted 6 July 2011
Available online 18 July 2011

Key words:
Nanoparticles
Tumor tissue slices
Telomerase
Inhibition
Oligonucleotide
Primary lung cells

ABSTRACT

Nanoparticles delivery of oligonucleotides represents a potential approach for cancer treatment. However, most of the experiments were based on established cancer cell lines and may not reflect the original solid tumor *in vivo*. Both, tumor microenvironment and tumor cell biological properties in the tumor can influence the delivery efficiency of oligonucleotides. Therefore, it is important to understand the effect of nanoparticles delivery of oligonucleotides on tumor response in intact tissue architecture of individual tumors. We used freshly isolated human tumor tissue slices and primary lung cancer cells from non-small cell lung cancer patients to evaluate this nanocarrier system. Chitosan-coated poly(lactide-co-glycolide) (PLGA) nanoparticles were used to form oligonucleotide–nanoparticle-complexes (nanoplexes) with antisense 2′-O-methyl-RNA (OMR) that can inhibit telomerase activity by binding to the RNA component of telomerase. OMR cellular uptake was strongly enhanced by nanoplexes mediated delivery in both, primary cells and tissue slices. More than 80% of primary cancer cells and 50% of cells in tissue slices showed OMR uptake. Telomerase activity was inhibited by approximately 45% in primary cancer cells and about 40% in tissue slices. Nanoplexes could penetrate into tumor tissue without influencing tissue architecture and the delivered OMR was able to inhibit telomerase activity with relatively low cytotoxicity.

1. Introduction

Antisense oligonucleotides have great potential for cancer treatment. However, the poor cellular uptake is a limiting factor that may contribute to the lack of functional efficacy in anticancer therapy (Akhtar and Juliano, 1992; Fattal and Barratt, 2009). Biodegradable nanoparticles have shown to be a promising drug delivery system. The cationic chitosan-coated poly(lactide-co-glycolide) (PLGA) nanoparticles are able to interact with oligonucleotides through electrostatic interaction to form nanoplexes that have relatively low cytotoxicity on the cells (Beisner et al., 2010; Nafee et al., 2007; Katas et al., 2008). Delivery of oligonucleotides, including tissue disposition, degradation and elimination are important factors for their efficacy *in vivo* (Agrawal, 1999). A solid tumor has a complex structure consisting of tumor cells, stromal cells and associated extracellular matrix (Tredan et al., 2007). This extracellular matrix forms a tight network that can hinder the penetration of drugs into tumors (Fattal and Barratt, 2009; Morin, 2003; Tannock et al., 2002) or affect the sensitivity of tumor cells to drugs (Dalton, 1999; Morin, 2003). Thus, the tumor microenvironment plays a role in drug resistance in tumor tissues (Morin, 2003). Therefore, it is important to understand the effect of nanoparticle mediated delivery of antisense oligonucleotides on tumor response in the intact tumor microenvironment of individual tumors.

The *ex vivo* tissue slice culture model as a three dimensional system has been used to investigate pharmacological properties of anticancer drugs (Sonnenberg et al., 2008; Umachandran and

* Corresponding author at: Dr. Margarete Fischer-Bosch-Institute of Clinical Pharmacology, University of Tübingen, Auerbachstraße 112, D-70376 Stuttgart, Germany. Tel.: +49 711 8101 5974; fax: +49 711 859295.
E-mail address: thomas.muerdter@ikp-stuttgart.de (T.E. Mürdter).
[1] Present address: Department of Pharmaceutics, Faculty of Pharmacy, Alexandria University, Alexandria, Egypt.

0378-5173/$ – see front matter © 2011 Elsevier B.V. All rights reserved.
doi:10.1016/j.ijpharm.2011.07.009

Ioannides, 2006; Vaira et al., 2010; van der Kuip et al., 2006). This model could maintain both organ and cellular architecture, keep the original cancer microenvironment and preserve the integrity of the tumor–stroma interaction (Umachandran and Ioannides, 2006; Vaira et al., 2010). The thin tissue slice (200 μm thickness) allows a smooth diffusion of oxygen, nutrients and antibodies. The cell viability in tissue slices can be maintained for at least 4 days under normal culture conditions (van der Kuip et al., 2006). This model presents a valid tool by which the anticancer drugs can be rapidly studied within the native tumor microenvironment of individual patients (Vaira et al., 2010).

Lung cancer is the leading cause of cancer death worldwide in both men and women (Jemal et al., 2010). Non-small cell lung cancer (NSCLC) is the main type and constitutes about 80% of all lung cancers. One promising approach to treat NSCLC is based on the inhibition of telomerase activity in cancer cells (Dong et al., 2010). Telomerase is an enzyme that adds telomeric repeats to the end of linear eukaryotic chromosomes. The human telomerase consists of a telomerase RNA (hTR), a telomerase reverse transcriptase (hTERT) and other associated proteins. The catalytic protein subunit hTERT uses hTR as a template for adding telomeric repeats to the telomere DNA strand (Blackburn, 1991). Telomerase is not active in most somatic cells but is expressed in human germ line cells, stem cells and many cancer cells. As a consequence of telomerase activity the cells can become immortal and keep dividing (Kim et al., 1994; Wright et al., 1996). Telomerase activity is detected in about 80% of NSCLC and is correlated with a poor prognosis (Hiyama et al., 1995; Taga et al., 1999). The telomerase RNA template hTR is an ideal target for inhibition by oligonucleotides (Harley, 2008; Philippi et al., 2010). The antisense oligonucleotide 2′-O-methyl-RNA (OMR) with a phosphorothioate backbone can specifically inhibit hTR leading to progressive telomere shortening (Herbert et al., 1999; Pitts and Corey, 1998).

Previously, we have demonstrated that delivery of antisense OMR with chitosan-coated PLGA nanoparticles induced efficient telomerase inhibition in human NSCLC cells (Beisner et al., 2010) and has a potential to be used as inhalation therapy. However, these results were based on established lung cancer cell lines and therefore may not totally reflect the behavior of tumor cells in original tumor tissues. In contrast, freshly isolated primary lung cancer cells in short-term culture retain many characteristics of cancer cells in primary tumors and show biological properties more closely related to the original tumors than cancer cell lines (Burdall et al., 2003). But it is still a two dimensional culture system and cannot reflect the solid tumor architecture as the tissue slice that can be used to study the tumor response to nanoparticle delivery systems in the complex environment of a primary cancer tissue. In the present study, we used freshly isolated human tumor tissue slices and primary lung cancer cells from NSCLC patients to evaluate the nanoparticle delivery of OMR and its biological effect on telomerase inhibition.

2. Material and methods

2.1. Lung tumor materials

Fresh tissues of primary NSCLC were obtained as surgical waste from patients newly diagnosed for NSCLC at the Klinik Schillerhöhe. Immediately after surgical resection, tumor tissues were maintained on ice until further processing. Fifteen tumor tissues were used for tissue slices preparation and 33 tumor tissues were used for isolation of primary lung cancer cells. The investigation was approved by the local ethics committee (#396/2005V) and informed consent was obtained from all patients.

2.2. Primary cells isolation, cultivation and characterization

The minced NSCLC tissue was enzymatically digested using a tissue disaggregation buffer (1 mM NaH_2PO_4, 5.4 mM KCl, 120 mM NaCl, 5.6 mM glucose, 2.5 mM $MgCl_2$, 20 mM HEPES, pH 7.2) supplemented with 167 U/ml collagenase, 250 U/ml DNase and 0.25 mg/ml protease for 90 min at 37 °C (Sonnenberg et al., 2008). The digested tissue suspension was passed through a 70 μm mesh nylon filter (BD Falcon) to remove cell clumps. Primary lung cancer cells were isolated from cell suspension using the magnetic-activated cell sorting (MACS) system. Cells were incubated with monoclonal CD326 (EpCAM) antibodies conjugated to microbeads (human Anti-HEA (Ep-CAM) Microbeads, Miltenyi Biotec, Bergisch Gladbach, Germany) for 30 min at 4 °C and passed through a positive selection column (MACS® Cell Seperation Column, Miltenyi Biotec, Bergisch Gladbach, Germany). CD326 positive cell populations were selected as primary lung cancer cells and cultivated with Airway Epithelial Cell Growth medium with Supplement Mix (PromoCell, Heidelberg, Germany), 50 μg/ml gentamicin (PromoCell, Heidelberg, Germany) and 0.05 μg/ml amphotericin B (PromoCell, Heidelberg, Germany) in Collagen IV 24-well plates (BD Biosciences, Bedford, USA). CD326 negative cells were cultured as primary lung fibroblasts in RPMI1640 medium supplemented with 20% heat inactivated fetal calf serum (FCS), 1 mM sodium pyruvate, 2 mM L-glutamine, 10 mM HEPES, 1% 2-mercaptoethanol, 0.5% non-essential amino acids (NEA, BioChromag, Berlin, Germany), 0.02 mg/ml asparagin, 50 U/ml penicillin and 50 μg/ml streptomycin. Cell viability was assessed by the trypan blue exclusion test. Primary cells were further identified by fluorescence-activated cell sorting (FACS) for epithelial specific antigen (ESA) expression.

2.3. Tissue slice preparation and cultivation

Preparation of tissue slices was performed as described previously (van der Kuip et al., 2006). Briefly, tissue slices (thickness: 200 μm, diameter: 5 mm) were cut by a Krumdieck microtome. Slices were individually submerged in the same medium used for primary lung cancer cell culture in 24-well plates. Each well contained one slice. Incubation was performed at 37 °C in a constant atmosphere of 5% CO_2. Treatment started 24 h after the preparation of the slices.

2.4. Oligonucleotides

The telomerase inhibitor is an antisense 2′-O-methyl-RNA(OMR) with a phosphorothioate(ps) backbone 5′-2′-O-methyl [C(ps)A(ps)GUUAGGGUU(ps)A(ps)G]-3′. The mismatch OMR is 5′-2′-O-methyl [C(ps)A(ps)GUUAGAAUU(ps)A(ps)G]-3′. The fluorescence-labeled OMR (FAM-OMR) is 5′-FAM-2′-O-methyl [C(ps)A(ps)GUUAGGGUU(ps)A(ps)G]-3′ and the digoxigenin-labeled OMR (Dig-OMR) is 5′-2′-O-methyl [C(ps)A(ps)GUUAGGGUU (ps)A(ps)G]-digoxigenin-3′. All oligonucleotides were synthesized by Biomers (Ulm, Germany). To ensure the stability and biological activity of the oligonucleotides, small aliquots were tested in the cell-free TRAP assay prior to use.

2.5. Preparation and characterization of chitosan-coated PLGA nanoparticles

Chitosan-coated PLGA nanoparticles were prepared by an emulsion–diffusion–evaporation method described previously (Kumar et al., 2004; Nafee et al., 2007). In brief, 5 ml of 2% PLGA (Polysciences Inc., Warrington, USA) were dissolved in ethyl acetate. The organic phase was added dropwise to 5 ml of an aqueous solution of 2.5% (w/v) stabilizer polyvinyl alcohol (Sigma Chemical Co., St. Louis, USA) and 0.3% (w/v) cationic polymer chitosan

(NovaMatrix, Drammen, Norway) under stirring and was further stirred for 1 h. The emulsion was homogenized using an UltraTurrax T25 (Janke & Kunkel GmbH & Co-KG, Staufen, Germany) for 10 min. MilliQ-water was added up to 50 ml to the homogenized emulsion. Organic solvent was removed by continuous stirring overnight at room temperature to obtain a suspension of nanoparticles.

Size, polydispersity index (PdI) and Zeta potential of nanoparticles were measured directly after preparation. Size of nanoparticles was in the range of 228–235 nm with a mean size (±SD) of 230 nm (±4 nm). The PdI was 0.13 (±0.054). The surface charge of nanoparticles measured as zeta potential was +32 mV (±6 mV). Nanoparticle concentration was determined gravimetrically after lyophilization to be 4.8 mg/ml (±0.79 mg/ml). Particles were further confirmed by atomic force microscopy as spherical with a monomodal size distribution.

2.6. Preparation of oligonucleotide–nanoparticle-complexes (nanoplexes) for transfection

Certain amounts of oligonucleotides were dissolved in cell culture medium to a final concentration of 4 μM. A suspension of nanoparticles was added and mixed. Then the mixture was incubated for 15 min at 37 °C to form oligonucleotide–nanoparticle-complexes (nanoplexes). The content ratio of nanoplexes was 1:50 ($weight_{oligonucleotide}/weight_{nanoparticles}$) for the treatment of primary cells and 1:100 ($weight_{oligonucleotide}/weight_{nanoparticles}$) for treatment of tissue slices. Primary cells and tissue slices were incubated with either OMR–nanoparticle-complexes (OMR-nanoplexes), OMR alone or mismatch-OMR–nanoparticle-complexes (mismatch-OMR-nanoplexes); either FAM-OMR alone or FAM-OMR–nanoparticle-complexes (FAM-OMR-nanoplexes); either Dig-OMR alone or Dig-OMR–nanoparticles-complexes (Dig-OMR-nanoplexes), separately. Six hours after treatment the mixture was replaced by cell culture medium. Tissue slices or primary cells were further cultured for 24 h or 72 h.

2.7. Fluorescence-activated cell sorting (FACS) analysis

For characterization, primary cells were incubated with anti-ESA-FITC (1:20; Biomeda, Foster City, CA) at room temperature for 20 min in the dark. For binding and/or uptake analysis, primary cells were collected and washed twice with PBS after treatment. The resuspended cell pellets were analyzed by FACScan fluorescence-activated cell sorter (Becton–Dickinson, Heidelberg, Germany) and 10,000 events were counted for each sample. Data were analyzed using CellQuest software (Becton–Dickinson, Heidelberg, Germany).

2.8. Confocal laser scanning microscopy (CLSM) analysis

Primary cells were treated either with FAM-OMR alone or FAM-OMR-nanoplexes one day after cells were seeded in Lab-Tek® chamber slides (Nalge Nunc International, Naperville, USA). Cells were observed at 6 h, 24 h and 72 h after treatment, respectively. After washing with PBS, cell membranes were stained with 25 μg/ml Rhodamine-labeled *Ricinus communis* Agglutinin I (RCA I, Vector Laboratories, Burlingame, CA, USA) for 15 min at 37 °C in the dark. Then cells were fixed with 100% ethanol at −20 °C for 10 min. The cell nuclei were stained with 1 μM TO-PRO®-3 iodide (Molecular Probes Invitrogen, Eugene, OR, USA) for 10 min at room temperature in the dark. Sections were mounted with mounting medium (Vectashield® Mounting Medium, Vector Laboratories, Burlingame, CA) for analyzing by CLSM.

One day after preparation of tissue slices, they were treated with either FAM-OMR alone or FAM-OMR-nanoplexes. Twenty-four hours and 72 h after treatment, tissue slices were washed with PBS and incubated with 25 μg/ml RCA I for 15 min at 37 °C. After washing with PBS, they were incubated with 6.25 μM DRAQ5™ (Biostatus Limited, Lörrach, Germany) for 10 min at room temperature in the dark and immediately examined by CLSM. Images were taken randomly from different areas. For every image taken, the efficiency of uptake in percent was calculated from the number of positive cells and the total cell number. A mean value of each sample was calculated from 12 images. All steps were performed without direct exposure to the light or in the dark to protect the fluorescence.

To identify cytotoxicity within the non-fixed tissue slices, we used a three-color fluorescent viability assay as described previously (van der Kuip et al., 2006). Briefly, tumor tissue slices were incubated simultaneously with 0.5 μM tetramethylrhodamine methyl ester perchlorate (TMRM, Sigma–Aldrich, Deisenhofen, Germany) and 5 μM DRAQ5™ for 20 min at 37 °C in the dark, followed by Picogreen (1:1500 dilution, Molecular Probes, Invitrogen) for additional 10 min at 37 °C in the dark and analyzed immediately without further washing steps using CLSM. Images were taken randomly from different areas. Cells which showed signals from Picogreen in the nuclei were considered as dead cells. For each image the viability was calculated by dividing the number of living cells by the total cell number. A mean value was calculated from 12 images. Experiments were repeated with tumor tissue slices from different patients.

CLSM was performed with a Leica LCS (Leica Lasertechnik, Heidelberg, Germany) instrument based on a Leica DM IRBE microscope equipped with argon and helium/neon lasers. The excitation (Ex.) and emission (Em.) wavelengths were as follows: Picogreen and FAM (Ex. 488 nm, Em. 500–540 nm); TMRM and RCA I (Ex. 543 nm, Em. 560–610 nm); TO-PRO®-3 and DRAQ5™ (Ex. 563 nm, Em. 650–700 nm).

2.9. Telomerase activity assay using real-time quantitative PCR

Primary cells were harvested and 500,000 cells were further pelleted and washed with PBS. The cell pellets were either stored at −80 °C or immediately resuspended in 100 μl ice-cold 3-[(3-cholamidopropyl)dimethyl-ammonio]-1-propanesulfonate (CHAPS) lysis buffer and incubated on ice for 30 min. Tissue slices were isolated using the FastPrep system: 300 μl CHAPS buffer with 200 U recombinant ribonuclease inhibitor (RNaseOUT™, Invitrogen, Carlsbad, CA) were added into a Lysing Matrix D tube with spheres (MP Biomedical, Solon, OH). Two frozen tissue slices were transferred into the tube and homogenized by a FastPrep® FP120 cell disrupter (Thermo Savant Bio101, Cedex, France) for 20 s at 4 °C. After short centrifugation the tubes were left on ice for another 30 min. The upper phase was transferred to a new tube and centrifuged at 12,000 × *g* for 20 min at 4 °C. The supernatants were aliquoted, snap-frozen and stored at −80 °C.

Telomerase activity was measured using an optimization of the modified real-time quantitative PCR based telomeric repeat amplification protocol (Q-TRAP) assay described by Herbert et al. (2006). Briefly, Q-TRAP reaction was performed in 384-well clear optical reaction plates (MicroAmp®, Applied Biosystems, USA) with a final reaction volume of 12 μl containing 2 μl cell extract (0.1 μg protein), 50 ng telomerase primer TS, 50 ng anchored return primer ACX and SYBR Green PCR Master Mix (QuantiTect®, QIAGEN, Hilden, Germany). Using the 7900HT Fast Real-Time PCR System (Applied Biosystems, USA) samples were incubated for 30 min at 30 °C for telomerase mediated extension reaction (if present), 95 °C for 1 min followed by 40 cycles of 94 °C for 15 s, 60 °C for 60 s. The threshold cycle value (*Ct*) of each sample was

determined from amplification log plots (the change in fluorescent signal was plotted against cycle number) and compared to standard curves. Calibration curves were generated from serial dilutions of telomerase-positive human lung cancer cell line A549 cell extracts with 1.0, 0.2, 0.04, 0.008 and 0.0016 μg of protein, respectively. The *Ct* values of calibration samples were plotted against log[protein] to calculate the linear equation. Negative control samples were created by heat inactivation at 85 °C for 10 min. Telomerase activity of each sample was expressed as relative telomerase activity (RTA) to A549 cells (telomerase activity of 1 μg protein of A549 cell extracts was defined as 1). Standards, inactivated samples and lysis-buffer controls were included in each Q-TRAP assay run. Primers were synthesized by Biomers (Ulm, Germany) with the following sequences: TS primer 5′-AATCCGTCGAGCAGAGTT-3′ and ACX primer 5′-GCGCGGCTTACCCTTACCCTTACCCTAACC-3′. All measurements were performed in triplicates.

2.10. Immunohistochemical staining

After treatment, tissue slices were fixed in 4% buffered formalin and embedded in paraffin for further investigation. The fixed tissue slices were cut in 3 μm serial sections by Rotary Microtome (Leica RM2255, Germany). Paraffin sections were stained with hematoxylin and eosin (HE) for histopathological examination. Immunohistochemical staining for KI67 (1:75, Monoclonal Mouse Anti-human KI67 Antigen, Clone MIB-1, Dakocytomation, Glostrup, Denmark) and hTERT (30 μg/ml, Rabbit Anti-hEst2 IgG, Alpha Diagnostic International, San Antonio, USA) were performed using the Dako Envision Kit according to the manufacturers manual. Immunohistochemical staining for Dig-OMR was performed using Mouse-anti-DIG antibody (ZytoVision, Bremerhaven, Germany). Epitope retrieval was achieved as follows: prior to staining with KI67 and mouse-anti-DIG, sections were treated for 30 min with citric acid buffer pH 6.0 (Dako, Glostrup, Denmark) in a steam heater. For hTERT staining, sections were treated for 15 min with Tris/EDTA buffer pH 9.0 (Dako, Glostrup, Denmark) in a pressure cooker. Counterstaining was performed with hematoxylin. Images were taken by a DigitalMicroscope (Leica DM 4000B) and analyzed by Leica Application SuiteV3. Immunohistochemical assessments were performed independently by two observers (MD, TM). The percentage of positive KI67 was calculated by relating the number of positive cells to the total cell number.

2.11. Statistical analysis

Different groups were compared by Wilcoxon signed rank test or Wilcoxon matched pairs test. Results were considered statistically significant if $p < 0.05$. All data were analyzed by Graphpad Prism version 4.0 (GraphPad Software Incorp., San Diego, CA).

3. Results

3.1. Cultivation and characterization of primary cells

The isolated cells were put into culture in an attempt to get primary lung cancer cells. The mean cell viability after isolation was 81.4% ± 11% (mean ± SD). From 9 out of the isolated 33 tissue samples, primary lung cancer cells proliferated and enough cells were obtained for further experiments after 3–5 passages. Telomerase activity was detected in 29 out of these 33 NSCLC specimens. Before treatment, cells were tested for the expression of ESA by FACS analysis (Fig. 1A). At least 75% of cells showed positive expression for ESA in the tested primary cells. The ESA positive cells were used for further studies.

3.2. Preparation and cultivation of tissue slices

Different numbers of viable tissue slices were obtained from 14 out of 15 telomerase positive primary lung cancer samples. In one case the tissue was contaminated with bacteria. Tissue slices from 8 telomerase positive samples were used for evaluating telomerase inhibition by the Q-TRAP assay. Six samples were applied for FAM-OMR uptake efficiency tests, 3 samples were used for Dig-OMR uptake efficiency tests, 6 samples were used for viability tests, 8 samples were used for immunohistochemical staining.

3.3. Nanoparticle delivery of 2′-O-methyl-RNA in primary lung cancer cells and tissue slices

FACS was used to quantify the binding and/or uptake of nanoplexes prepared with FAM-OMR in human primary lung cancer cells and fibroblasts 24 h after treatment. The treatment of cells with FAM-OMR-nanoplexes revealed a markedly stronger shift in the fluorescence profile of the cell population reflecting a higher cell binding and/or uptake compared to OMR alone in both primary lung cancer cells and fibroblasts (Fig. 1B). The percentage of cells above the fluorescence threshold was 90.9 ± 2.8% (mean ± SD, $n = 3$) for primary lung cancer cells and 99.1 ± 1.1% (mean ± SD, $n = 3$) for fibroblasts. The cell population showed a slight shift with FAM-OMR in the absence of nanoparticles in both cell types and this shift was more pronounced in primary lung cancer cells compared to fibroblasts (Fig. 1B). Compared to the dramatic shift after FAM-OMR-nanoplexes treatment, the population shift after FAM-OMR treatment was negligible and might be caused by unspecific binding. As expected, treatment with nanoparticles alone did not show any effects.

The localization of FAM-OMR in primary cells and tissue slices was determined by CLSM. The uptake of nanoplexes into cells appeared to be a stepwise process. In primary lung cancer cells, the FAM-OMR was accumulated on the membrane of cells after 6 h of treatment (Fig. 1C). Only few cells showed an uptake of FAM-OMR, less than 5% of cells exhibited fluorescence in nuclei. An uptake into the primary cells was observed 24 h after treatment; the FAM-OMR appeared inside the cells and was mainly located in the cytoplasm as small spots in the perinuclear area (Fig. 1D). Seventy-two hours after treatment more than 80% of cells displayed fluorescence signals within the cells and approximately 20% of these cells within the nuclei (Fig. 1E). CLSM proved that the high fluorescence intensities in FAM-OMR-nanoplexes treated primary lung cancer cells as observed by FACS is due to an intracellular uptake rather than an adsorption of nanoplexes to the cell surface. In primary lung fibroblasts, the FAM-OMR accumulated mostly on the cell membranes during the whole observation time. The fluorescence signal localization showed almost no difference 6 h, 24 h, and 72 h after transfection (Fig. 1F–H). Although primary lung fibroblasts treated with FAM-OMR-nanoplexes demonstrated high fluorescence intensities by FACS analysis, the cells did not show uptake of nanoplexes in CLSM; thus the fluorescence signal is due to an adsorption of nanoplexes to the cell surface.

In tumor tissue slices, the uptake of nanoplexes started after 6 h of treatment (data not shown), more than 50% of cells exhibited uptake in the following incubation times (Fig. 2C–F). The OMR-nanoplexes were able to penetrate the whole tissue slice and showed equally distribution at different depths and areas (Supplementary file 1). Interestingly, the uptake of FAM-OMR-nanoplexes displayed a spotted distribution within the nuclei, which is different to the uptake into primary lung cancer cells. Nanoplexes significantly enhanced efficiency of uptake.

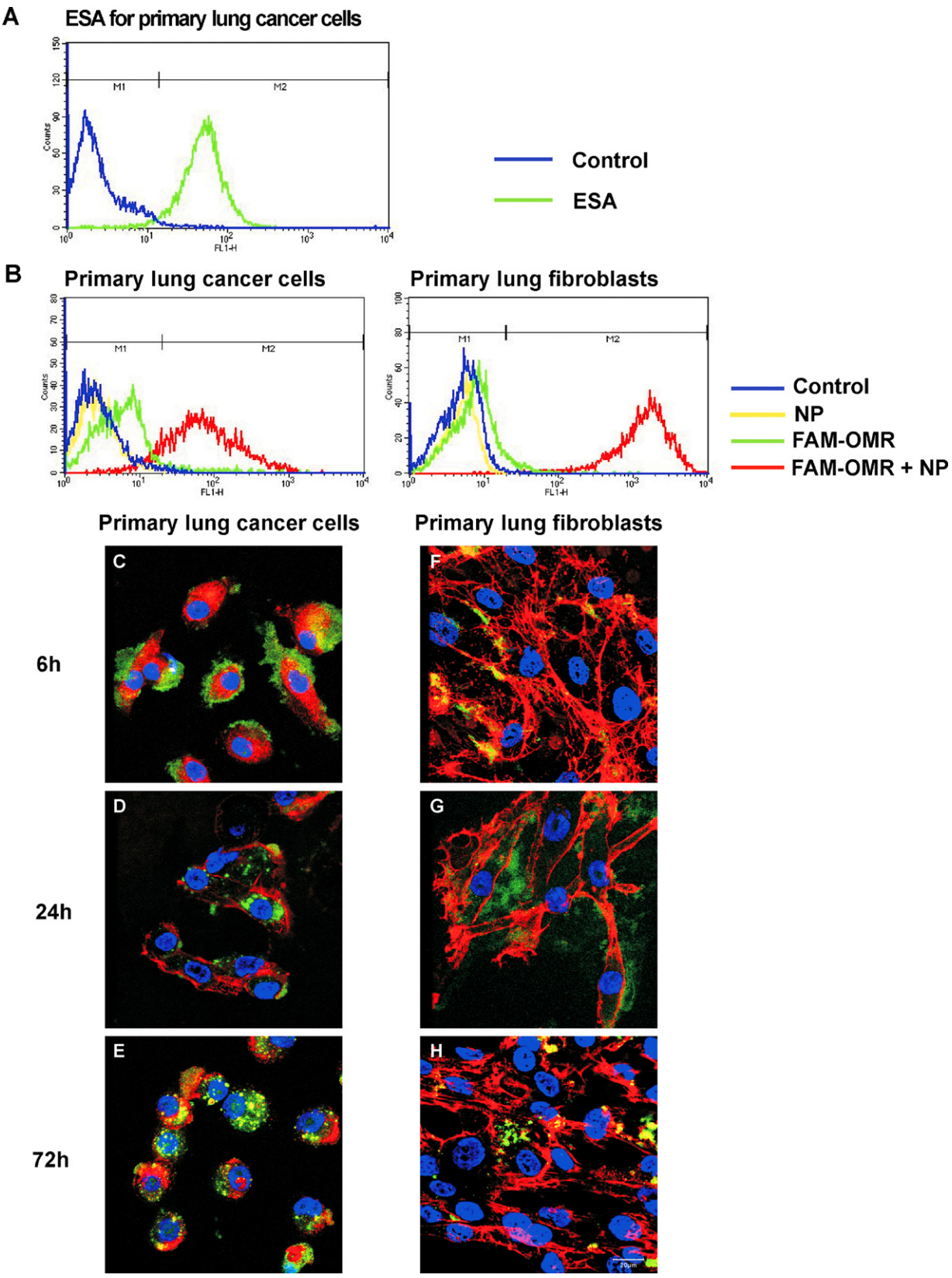

Fig. 1. (A) FACS analysis of human lung cancer cells for epithelial specific antigen (ESA) expression. Experiments were performed for each cultured primary lung cancer cells and a representative experiment is shown. (B) Uptake of 2′-O-methyl-RNA in primary lung cancer cells and primary lung fibroblasts analyzed by FACS 24 h after treatment with FAM-labeled 2′-O-methyl-RNA alone (FAM-OMR), nanoparticles alone (NP) or FAM-labeled 2′-O-methyl-RNA-nanoplexes (FAM-OMR + NP). The corresponding non-treated primary cells were used as control. Experiments were repeated 3 times with different primary cells and a representative experiment is shown. (C–H) Localization of nanoparticles delivered FAM-labeled 2′-O-methyl-RNA (green) in primary lung cancer cells (C–E) and primary lung fibroblasts (F–H) visualized by confocal laser scanning microscopy. Cell membranes were stained with RCA I (red) and nuclei with TO-PRO®-3 (blue) before microscopic observation (63× objective). Scale bar represents 20 μm.

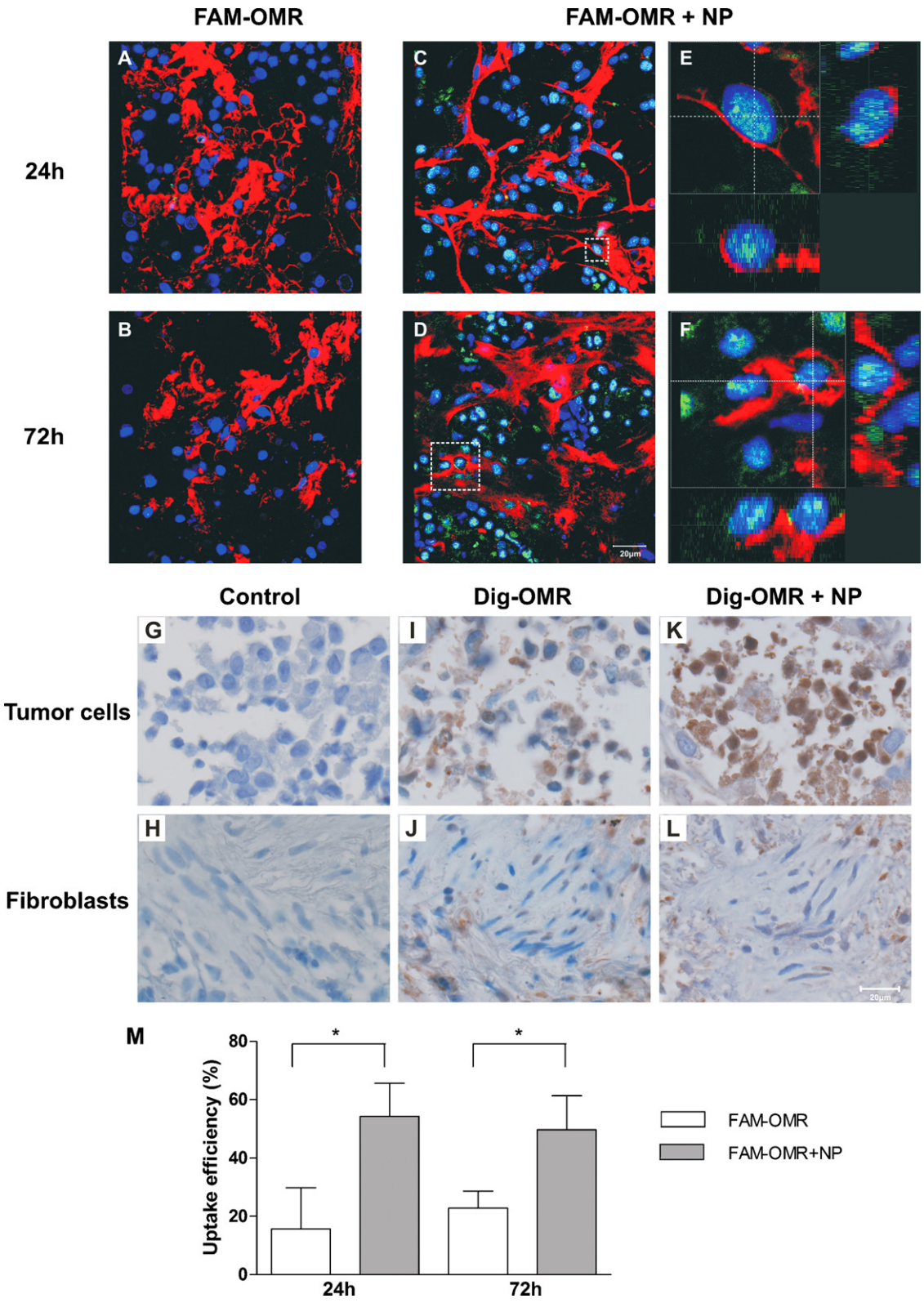

Fig. 2. (A–F) Localization of nanoparticles delivered FAM-labeled 2′-O-methyl-RNA (green) in cells of tissue slices visualized by confocal laser scanning microscopy. Images were taken 24 h and 72 h after treatment with (A and B) FAM-labeled 2′-O-methyl-RNA (FAM-OMR); (C and D) FAM-labeled 2′-O-methyl-RNA-nanoplexes (FAM-OMR + NP). (E and F) Shows the transverse and vertical sections of a single cell zoomed out from (C and D), respectively. Cell membranes were stained with RCA I (red) and nuclei with DRAQ5™ (blue) before microscopic observation (63× objective). Scale bar represents 20 μm. (G–L) Localization of nanoparticles delivered digoxigenin-labeled 2′-O-methyl-RNA in cells of tissue slices visualized by immunohistochemistry with mouse-anti-DIG antibody and counterstained with hematoxylin (100× objective). Images of paraffin embedded tissue slices were taken 72 h after treatment with (I and J) digoxigenin-labeled 2′-O-methyl-RNA (Dig-OMR); (K and L) digoxigenin-labeled 2′-O-methyl-RNA-nanoplexes (Dig-OMR+NP). (G, I and K) are areas mainly containing tumor cells. (H, J and L) are areas mainly containing fibroblasts. Scale bar represents 20 μm. (M) Uptake efficiency of FAM-labeled 2′-O-methyl-RNA-nanoplexes in human lung tissue slices of different patients. For each tissue slice, images were taken from 12 different areas by confocal laser scanning microscopy and with each area at least 20 cells were counted. Uptake efficiency is given as % positive cells of total number of cells. Data represent the mean + SD from 6 independent experiments (*$p < 0.05$).

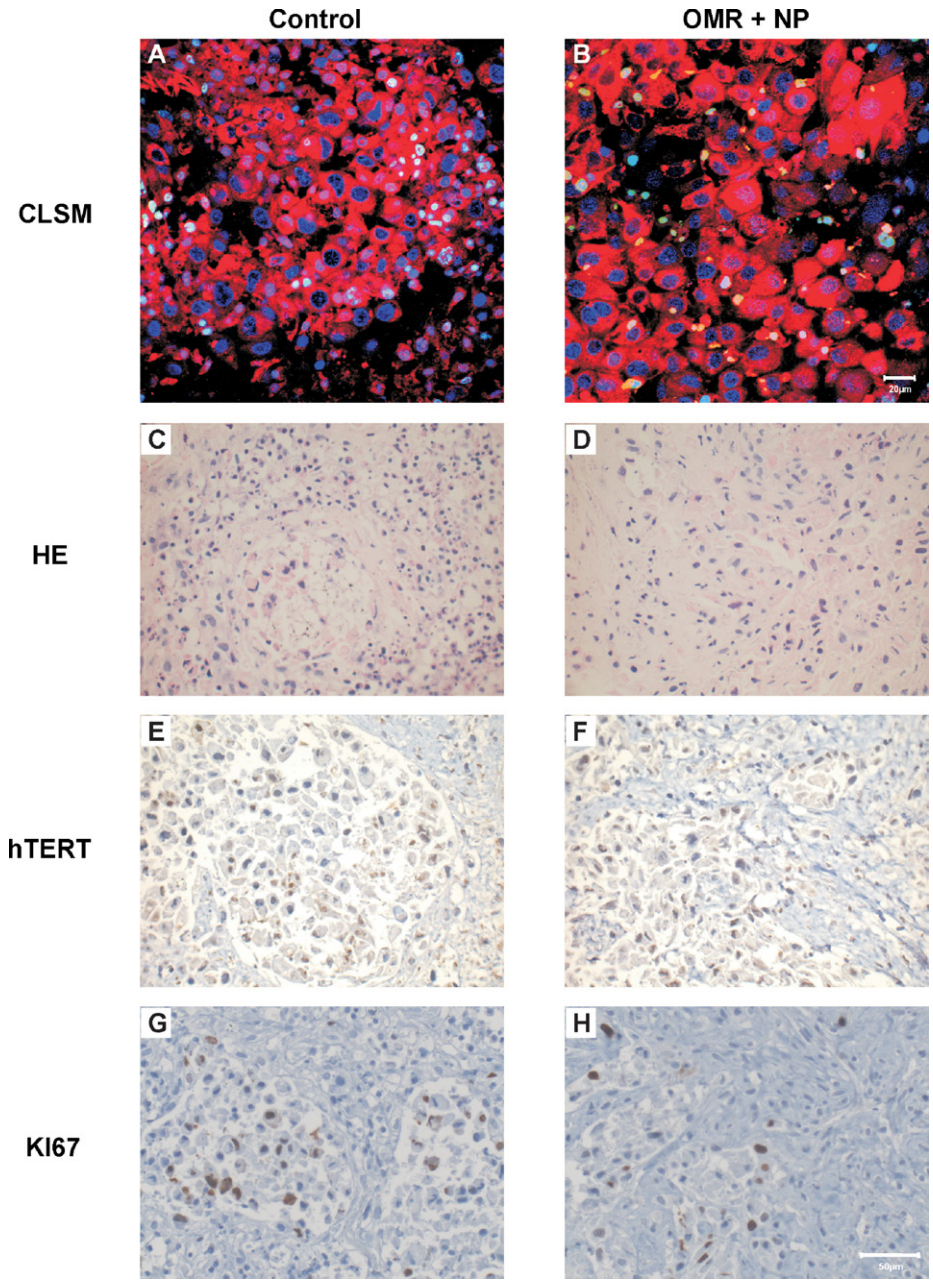

Fig. 3. Influence of 2′-O-methyl-RNA-nanoplexes on cell viability, morphology, proliferation and telomerase expression in human tissue slices 72 h after treatment with 2′-O-methyl-RNA-nanoplexes (OMR + NP). Untreated tissue slices were used as control. (A and B) Cell viability in tissue slices was determined by confocal laser scanning microscopy (CLSM). Living cells were stained with TMRM (red) and dead cells with Picogreen (green). All cell nuclei were stained with DRAQ5™ (blue) before microscopic observation (40× objective). Scale bar represents 20 μm. (C–H) Representative examples of sections from paraffin embedded tissue slices stained with hematoxylin and eosin (HE) for cell morphology (C and D); Anti-hEst2 IgG antibody for human telomerase reverse transcriptase (hTERT) expression (E and F); KI67 for cell proliferation (G and H) (40× objective). Scale bar represents 50 μm.

Compared to FAM-OMR-nanoplexes, uptake of FAM-OMR alone was only minor and did not improve over time (Fig. 2A and B). There was a significant difference for the uptake efficiency between treatment with FAM-OMR alone and with FAM-OMR-nanoplexes both, 24 h and 72 h after treatment (Fig. 2M). The results were further confirmed by immunohistochemical staining for nanoparticles delivery of Dig-OMR in tissue slices. The tissue slices treated with Dig-OMR-nanoplexes exhibited much more digoxigenin signal than tissue slices treated only with Dig-OMR (Fig. 2I and K). Interestingly, the digoxigenin signal was mainly present in the tumor cells but not in stromal cells indicating that tumor cells showed nanoparticle mediated uptake of Dig-OMR (Fig. 2G–L).

3.4. Cytotoxicity of nanoparticles delivery of 2′-O-methyl-RNA

After treatment with nanoplexes, viability of primary lung cancer cells was reduced by 30 ± 12% if compared to untreated controls. There was no difference in cytotoxicity among the treatments with OMR-nanoplexes, mismatch-OMR-nanoplexes and nanoparticles alone. Compared to established cancer cell lines, primary lung cancer cells were more sensitive to the culture condition and the treatment. The slight cytotoxic effects were mainly caused by the treatment with nanoparticles not by the transfected oligonucleotides. To limit this effect, we decided to use nanoplexes prepared with a ratio of 1:50 instead of 1:100 ($weight_{oligonucleotide}/weight_{nanoparticles}$) for primary cells. As all

experiments were carried out with 4 μM OMR, the amount of nanoparticles used was halved.

In Fig. 3A and B viable cells displayed red fluorescence of TMRM which binds to active mitochondrial membranes, whereas nuclei of dead cells showed green fluorescence from Picogreen. Nuclei of cells were stained with DRAQ5™, which is a cell membrane permeable DNA-interactive agent. A high percentage of living cells was identified in tissue slices 72 h after treatment and no difference was found between nanoplexes treated specimens and the untreated controls. This was confirmed by quantification of Picogreen negative cells in relation to total cells in 6 different tumor samples. The mean ratio of living cells was more than 80% and no significant difference was seen for viability between both groups (data not shown) indicating that treatment with nanoplexes did not have an acute cytotoxic effect on the tissue slices.

3.5. Impact of 2′-O-methyl-RNA-nanoparticle-complexes on cell proliferation and telomerase expression in tissue slices

Hematoxylin and eosin (HE) histological examination of paraffin embedded tissue slices demonstrated that there was no obvious difference in the morphology between nanoplexes treated and untreated tissue slices 72 h after treatment (Fig. 3C and D). Nuclear hTERT expression was detected by immunohistochemistry in tissue slices with or without nanoplexes treatment using an affinity purified antibody which binds to a 16 amino acid peptide sequence within hTERT. After 72 h of cultivation, immunohistochemical staining indicated positive hTERT expression in tissue slices (Fig. 3E and F). The cell proliferation in tissue slices was analyzed using proliferation marker KI67 (Fig. 3G and H). The cell morphology and the expression of hTERT did not exhibit any difference between nanoplexes treated and control tissue slices. However, there was a trend towards a decrease of KI67-positive tumor cells following treatment with nanoplexes.

3.6. Inhibition of telomerase activity by 2′-O-methyl-RNA–nanoparticle-complexes in primary lung cancer cells and tissue slices

The Q-TRAP assay allows a more rapid and quantitative determination of telomerase activity in cells or tissue extracts. We modified this method to be of low-cost and high-throughput using 384-well reaction plates with only 12 μl total PCR reaction volume.

In primary cells, following treatment with OMR-nanoplexes telomerase activity was inhibited by approximately 45% ($p = 0.0313$). Treatment with mismatch-OMR-nanoplexes led only to a slight reduction of telomerase activity indicating a specific inhibition of telomerase by the OMR-nanoplexes (Fig. 4A).

Tissue slices from 8 different telomerase positive tumor samples were treated for 6 h with OMR alone or OMR-nanoplexes. Twenty-four hours after treatment with OMR-nanoplexes telomerase activity was reduced by about 40% ($p = 0.0078$) in tumor tissue slices. The group treated with OMR alone only showed about 15% inhibition of telomerase activity ($p = 0.0156$) (Fig. 4B). Treatment with nanoparticles alone did not exhibit significant telomerase inhibition effect on tumor tissue slices.

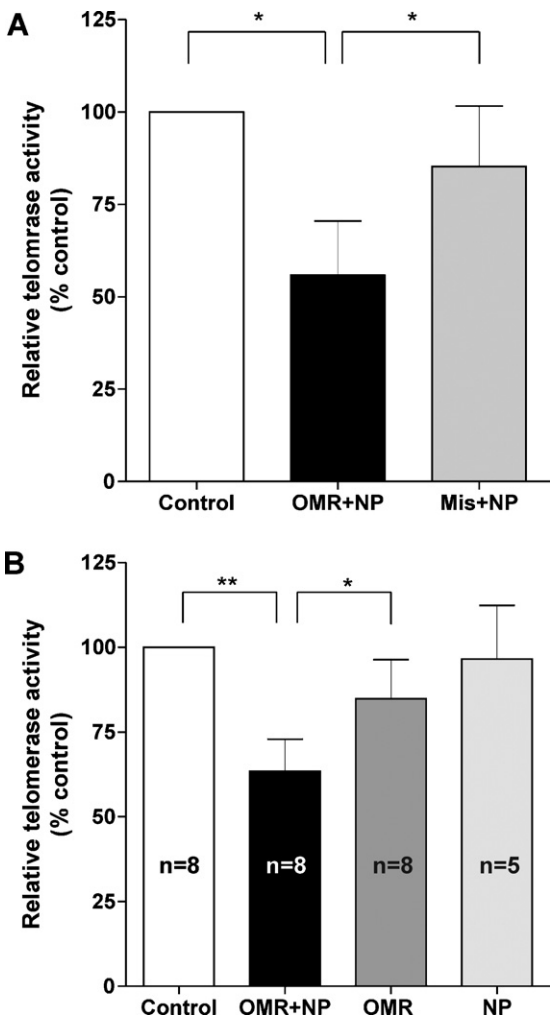

Fig. 4. (A) Inhibition of telomerase activity by nanoparticle delivery of 2′-O-methyl-RNA in primary lung cancer cells 72 h after treatment with either 2′-O-methyl-RNA-nanoplexes (OMR + NP) or mismatch-OMR-nanoplexes (Mis + NP). Telomerase activity of treated cells was normalized to corresponding untreated control cells. Data represent the mean + SD from 6 independent experiments (*$p < 0.05$). (B) Inhibition of telomerase activity by nanoparticle delivery of 2′-O-methyl-RNA in lung tissue slices 24 h after treatment with 2′-O-methyl-RNA alone (OMR), nanoparticles alone (NP) or 2′-O-methyl-RNA-nanoplexes (OMR + NP). Telomerase activity of treated tissue slices was normalized to corresponding untreated control tissue slices. Data represent the mean + SD from 8 different tumor specimens (**$p < 0.01$; *$p < 0.05$, $n = 5$ for NP treated group, $n = 8$ for all the other groups).

4. Discussion

In contrast to normal cells, tumor cells have relatively short telomeres but high telomerase activity (Zimmermann and Martens, 2007). This makes the inhibition of telomerase an interesting option for anticancer therapy. The efficient inhibition of telomerase can drive tumor cells into apoptosis, while telomerase negative normal somatic cells are not targeted and affected. Other telomerase positive cells, such as germ line cells and stem cells, also remain unaffected because of their longer telomere lengths and slower cell division rates (Shay and Wright, 2006; Zimmermann and Martens, 2007). It has been shown that OMR acts as a specific telomerase inhibitor and chitosan-coated PLGA nanoparticles enhance the delivery of OMR inducing telomerase inhibition and telomere length shortening in human NSCLC cells (Beisner et al., 2009, 2010). Since the cancer cell lines may contain genotypic and phenotypic drift (Burdall et al., 2003), we used primary lung cancer cells and tumor tissue slices in the present study to evaluate the telomerase inhibition by nanoparticle delivery of OMR.

Primary lung cancer cells were directly isolated from the tumor lesions. In order to establish a primary lung cancer cell culture that is suitable for *in vitro* experiments, we used collagen IV coated wells to improve cell attachment and airway epithelial cell culture medium to keep their characteristics. Nevertheless, the primary cancer cells within this culture system had only limited lifespan and slower population doubling times compared to established cancer cell lines. In addition, these primary cancer cells

were more sensitive to the condition of culture and environmental changes. Especially during the transfection procedure when cells were treated with nanoplexes or nanoparticles, cell viability decreased. We therefore reduced the amount of nanoparticles during treatments and increased the content ratio of nanoplexes from 1:100 to 1:50 ($weight_{oligonucleotide}/weight_{nanoparticles}$). Under these conditions, the experiments can be performed without remarkable decrease of cell viability. Telomerase activity of primary cancer cells was inhibited by about 40% after treatment with OMR-nanoplexes at a ratio of 1:50, which was comparable to A549 cells treated with OMR-nanoplexes at a ratio of 1:100 (Beisner et al., 2010). The original telomerase activities of these primary cells were highly variable within specimens. Cells that expressed high telomerase activity had a relative longer lifespan.

In our study, comparison of the morphology of the original tumor tissue with tissue slices by HE staining showed that neither the slicing procedure nor the treatment with nanoplexes changed the architecture of the tissue. In concordance, proliferation marker KI67 staining demonstrated only a slight difference in the fraction of proliferating tumor cells between treated slices and the control group after 72 h of incubation time. This is in agreement with the lack of acute toxicity of nanoplexes in lung cancer cell lines (Beisner et al., 2010). In long-term experiments, the population doublings of A549 cells was reduced by about 40% after 2 weeks treatment, but no obvious difference could be observed at the first 3 days (Beisner et al., 2010). This was expected as shortening of telomeres is a stepwise process needing several cell cycles to affect proliferation rate. The antisense OMR only targets the telomerase RNA template without interfering with transcriptional regulation of hTR (Pitts and Corey, 1998), it inhibits telomerase activity by competing with the telomeres but does not influence the hTERT expression. Since the mismatch OMR that contains two mismatched bases exhibited only a slight reduction of telomerase activity in A549 cells (Beisner et al., 2010) and primary lung cancer cells, the telomerase inhibition was sequence-dependent. Therefore, the effect of mismatch OMR on telomerase activity in the slice model was not studies.

Tissue slices from different NSCLC patients showed a broad distribution of telomerase activities. But the inhibition ratio of OMR-nanoplexes treatment did not demonstrate significant differences. The averaged telomerase inhibition was $36.5 \pm 9.4\%$ ($\pm$SD) indicating that the treatment worked successfully on different levels of telomerase activity. Among the different components of tumor tissue, only tumor cells exhibit high telomerase activity. When comparing telomerase activity of freshly isolated cancer cells to tumor tissue homogenates, the isolated cancer cells showed higher telomerase activity. This is explained by the fact that telomerase activity determined in tumor tissue slices was the average of tumor cells with high telomerase activity and stromal cells with undetectable telomerase.

Although primary lung fibroblasts exhibited high fluorescence intensities by FACS analysis after treatment with FAM-OMR-nanoplexes, the results of CLSM proved that these signals mostly came from the adsorption of nanoplexes to the cell surface. The results of immunohistochemical staining for tissue slices following treatment with Digo-OMR-nanoplexes also demonstrated that the digoxigenin signal was mainly present in the tumor cells not the stromal cells indicating that stromal cells showed only a low uptake rate of nanoplexes. This might explain that viability of primary lung fibroblasts was not affected by the treatment of nanoplexes (Beisner et al., 2010).

The *in vitro* cell line model is widely used to study molecular mechanisms of drug actions. It is easy to handle, highly reproducible with unlimited availability to repeat experiments and the cells are homogenous. However, cell morphology, cell–cell, cell–matrix and tumor–stroma interactions are different in these cell lines compared to tumor tissue (van der Kuip et al., 2006) and these interactions are extremely specific for each individual tumor *in vivo* (Morin, 2003). Although more closely related to the original tumor tissue than cell lines, primary cancer cell culture is still a two dimensional culture system and lacks most of these interactions. Furthermore, as these cells grow in a mono-layer, even large therapeutic molecules such as proteins or nanoparticles have easy access to the cell surface without any diffusion restrictions which may play a major role for the local availability of such drugs *in vivo*. For a successful treatment of solid tumors *in vivo*, nanoplexes have to penetrate the tumor tissue to affect all tumor cells. Within the tumor tissue, the complex tumor microenvironment may hamper the way of nanoplexes into tumor cells. The three dimensional *ex vivo* tissue culture model using tissue slices from primary human tumors can maintain both tumor and cellular architecture, keep the original tumor microenvironment, and preserve the complexity of the tumor–stroma interactions. The tumor tissue slices recover from the preparation process within 24 h and are fully viable for at least 4 days under normal culture conditions (Umachandran and Ioannides, 2006; van der Kuip et al., 2006; Vaira et al., 2010). Using this model we could proof that nanoplexes were able to permeate into the complete tumor tissue slice which has a thickness of 200 μm and lead to an inhibition of telomerase activity of tumor cells as efficient as in the primary cancer cell culture. The immunohistochemical staining for Dig-OMR delivered by nanoparticles exhibited comparable results to that obtained by CLSM using FAM-OMR. This further proved that the fluorescence-labeling of OMR was stable over the incubation time of 72 h and the self-quenching of fluorescence had no significant impact on the CLSM results. Taking into account the architecture of solid tumors with their vascularization the diffusion path into the tissue slices exceeds the distance from any viable tumor area to the nearest blood vessel. However, during surgery and tissue slice preparation, the vascular system of the tumor is disconnected from systemic blood flow and subsequently vessels in the tumor tissue collapse. Therefore, this tissue slice model cannot provide information on the penetration of drugs through the vessel wall into the extracellular space of the tumor. A major advantage of this model is the preparation of multiple tumor tissue slices from one tumor specimen. These enable the investigation of pharmacological properties of a series of anticancer drugs under various conditions in both, the preclinical and clinical settings.

The *in vivo* animal model can mimic the native environment for the tumors. Human tumor xenografts are the most commonly used models that allow either human cancer cells or tumor fragments to grow in the immune-deficient mouse (Nyga et al., 2011) enabling intervention studies during tumor growth over several weeks. On the other hand, the injection of a fast growing human tumor cell line into the mouse can lead to artificial tumor architecture with a low percentage of stromal cells within the tumor. In addition, there are certain differences between human and mouse cells, e.g. differences in growth factor or cytokine signaling may lead to differences in growth behavior, metastatic potential and sensitivity against drugs. Noteworthy, to obtain the required statistical power many animals need to be sacrificed. In summary, these different models have their own strengths and limitations. The tissue slice model provides a tool that can fill the gap between results based on monolayer culture of cancer cell lines and the reality in human solid tumors.

Our study showed that chitosan-coated PLGA nanoparticles exhibited high delivery efficiency of antisense oligonucleotide OMR into tumor cells with low cytotoxicity in three dimensional tissue structures. Comparable nanoparticles have been used to deliver small interfering RNA to human embryonic kidney cells without acute cytotoxic effects (Katas et al., 2008). Therefore, the results of the present study are not only of interest for the delivery of an

inhibitor of telomerase in cancer patients but also for the down regulation of gene expression as a more general application.

5. Conclusions

Inhibition of telomerase in tumor cells holds a promising approach in the treatment of solid tumors. Nanoparticle delivery of OMR can inhibit telomerase activity in the primary cancer cells isolated from NSCLC. Using the tissue culture model we could prove that (I) OMR-nanoplexes penetrate into tumor tissue, (II) transfect tumor cells in their "natural" environment to deliver OMR and (III) that telomerase activity of these cells is inhibited by this OMR. Therefore, the tissue slice model of human lung cancer appears to be a useful tool for translating nanotechnology based delivery of telomerase inhibitor antisense oligonucleotides into more complex *in vivo* experiments.

Acknowledgements

We are grateful to Mrs. S. Rekersbrink for excellent technical assistance and to Mrs. Silke Haubeiß and Mr. Jens Schmid for collaboration in primary cell isolation and tissue slice preparation in this study. This work was supported by the German Cancer Aid, Bonn (grant no. 107541), the German Federal Ministry of Education and Research, Berlin (grant no. 0315280C), and the Robert Bosch Foundation, Stuttgart, Germany.

Appendix A. Supplementary data

Supplementary data associated with this article can be found, in the online version, at doi:10.1016/j.ijpharm.2011.07.009.

References

Agrawal, S., 1999. Importance of nucleotide sequence and chemical modifications of antisense oligonucleotides. Biochim. Biophys. Acta 1489, 53–68.
Akhtar, S., Juliano, R.L., 1992. Cellular uptake and intracellular fate of antisense oligonucleotides. Trends Cell Biol. 2, 139–144.
Beisner, J., Dong, M., Taetz, S., Nafee, N., Griese, E.U., Schaefer, U., Lehr, C.M., Klotz, U., Murdter, T.E., 2010. Nanoparticle mediated delivery of 2′-O-methyl-RNA leads to efficient telomerase inhibition and telomere shortening in human lung cancer cells. Lung Cancer 68, 346–354.
Beisner, J., Dong, M., Taetz, S., Piotrowska, K., Kleideiter, E., Friedel, G., Schaefer, U., Lehr, C.M., Klotz, U., Murdter, T.E., 2009. Efficient telomerase inhibition in human non-small cell lung cancer cells by liposomal delivery of 2′-O-methyl-RNA. J. Pharm. Sci. 98, 1765–1774.
Blackburn, E.H., 1991. Telomeres. Trends Biochem. Sci. 16, 378–381.
Burdall, S.E., Hanby, A.M., Lansdown, M.R., Speirs, V., 2003. Breast cancer cell lines: friend or foe? Breast Cancer Res. 5, 89–95.
Dalton, W.S., 1999. The tumor microenvironment as a determinant of drug response and resistance. Drug Resist. Updat. 2, 285–288.
Dong, M., Murdter, T.E., Klotz, U., 2010. Telomeres and telomerase as novel drug targets: reflections on the 2009 Nobel Prize in Physiology or Medicine. Eur. J. Clin. Pharmacol. 66, 1–3.
Fattal, E., Barratt, G., 2009. Nanotechnologies and controlled release systems for the delivery of antisense oligonucleotides and small interfering RNA. Br. J. Pharmacol. 157, 179–194.
Harley, C.B., 2008. Telomerase and cancer therapeutics. Nat. Rev. Cancer 8, 167–179.
Herbert, B., Pitts, A.E., Baker, S.I., Hamilton, S.E., Wright, W.E., Shay, J.W., Corey, D.R., 1999. Inhibition of human telomerase in immortal human cells leads to progressive telomere shortening and cell death. Proc. Natl. Acad. Sci. U. S. A. 96, 14276–14281.
Herbert, B.S., Hochreiter, A.E., Wright, W.E., Shay, J.W., 2006. Nonradioactive detection of telomerase activity using the telomeric repeat amplification protocol. Nat. Protoc. 1, 1583–1590.
Hiyama, K., Hiyama, E., Ishioka, S., Yamakido, M., Inai, K., Gazdar, A.F., Piatyszek, M.A., Shay, J.W., 1995. Telomerase activity in small-cell and non-small-cell lung cancers. J. Natl. Cancer Inst. 87, 895–902.
Jemal, A., Siegel, R., Xu, J., Ward, E., 2010. Cancer statistics, 2010. CA Cancer J. Clin. 60, 277–300.
Katas, H., Chen, S., Osamuyimen, A.A., Cevher, E., Alpar, H.O., 2008. Effect of preparative variables on small interfering RNA loaded poly(D,L-lactide-co-glycolide)-chitosan submicron particles prepared by emulsification diffusion method. J. Microencapsul. 25, 541–548.
Kim, N.W., Piatyszek, M.A., Prowse, K.R., Harley, C.B., West, M.D., Ho, P.L., Coviello, G.M., Wright, W.E., Weinrich, S.L., Shay, J.W., 1994. Specific association of human telomerase activity with immortal cells and cancer. Science 266, 2011–2015.
Kumar, M.N., Mohapatra, S.S., Kong, X., Jena, P.K., Bakowsky, U., Lehr, C.M., 2004. Cationic poly(lactide-co-glycolide) nanoparticles as efficient in vivo gene transfection agents. J. Nanosci. Nanotechnol. 4, 990–994.
Morin, P.J., 2003. Drug resistance and the microenvironment: nature and nurture. Drug Resist. Updat. 6, 169–172.
Nafee, N., Taetz, S., Schneider, M., Schaefer, U.F., Lehr, C.M., 2007. Chitosan-coated PLGA nanoparticles for DNA/RNA delivery: effect of the formulation parameters on complexation and transfection of antisense oligonucleotides. Nanomedicine 3, 173–183.
Nyga, A., Cheema, U., Loizidou, M., 2011. 3D tumour models: novel in vitro approaches to cancer studies. J. Cell Commun. Signal..
Philippi, C., Loretz, B., Schaefer, U.F., Lehr, C.M., 2010. Telomerase as an emerging target to fight cancer – opportunities and challenges for nanomedicine. J. Control. Release 146, 228–240.
Pitts, A.E., Corey, D.R., 1998. Inhibition of human telomerase by 2′-O-methyl-RNA. Proc. Natl. Acad. Sci. U. S. A. 95, 11549–11554.
Shay, J.W., Wright, W.E., 2006. Telomerase therapeutics for cancer: challenges and new directions. Nat. Rev. Drug Discov. 5, 577–584.
Sonnenberg, M., van der Kuip, H., Haubeis, S., Fritz, P., Schroth, W., Friedel, G., Simon, W., Murdter, T.E., Aulitzky, W.E., 2008. Highly variable response to cytotoxic chemotherapy in carcinoma-associated fibroblasts (CAFs) from lung and breast. BMC Cancer 8, 364.
Taga, S., Osaki, T., Ohgami, A., Imoto, H., Yasumoto, K., 1999. Prognostic impact of telomerase activity in non-small cell lung cancers. Ann. Surg. 230, 715–720.
Tannock, I.F., Lee, C.M., Tunggal, J.K., Cowan, D.S., Egorin, M.J., 2002. Limited penetration of anticancer drugs through tumor tissue: a potential cause of resistance of solid tumors to chemotherapy. Clin. Cancer Res. 8, 878–884.
Tredan, O., Galmarini, C.M., Patel, K., Tannock, I.F., 2007. Drug resistance and the solid tumor microenvironment. J. Natl. Cancer Inst. 99, 1441–1454.
Umachandran, M., Ioannides, C., 2006. Stability of cytochromes P450 and phase II conjugation systems in precision-cut rat lung slices cultured up to 72 h. Toxicology 224, 14–21.
Vaira, V., Fedele, G., Pyne, S., Fasoli, E., Zadra, G., Bailey, D., Snyder, E., Faversani, A., Coggi, G., Flavin, R., Bosari, S., Loda, M., 2010. Preclinical model of organotypic culture for pharmacodynamic profiling of human tumors. Proc. Natl. Acad. Sci. U. S. A. 107, 8352–8356.
van der Kuip, H., Murdter, T.E., Sonnenberg, M., McClellan, M., Gutzeit, S., Gerteis, A., Simon, W., Fritz, P., Aulitzky, W.E., 2006. Short term culture of breast cancer tissues to study the activity of the anticancer drug taxol in an intact tumor environment. BMC Cancer 6, 86.
Wright, W.E., Piatyszek, M.A., Rainey, W.E., Byrd, W., Shay, J.W., 1996. Telomerase activity in human germline and embryonic tissues and cells. Dev. Genet. 18, 173–179.
Zimmermann, S., Martens, U.M., 2007. Telomeres and telomerase as targets for cancer therapy. Cell. Mol. Life Sci. 64, 906–921.